New Journal of Physics
The open access journal at the forefront of physics

Deutsche Physikalische Gesellschaft DPG IOP Institute of Physics

PAPER • OPEN ACCESS

Heating in multi-layer targets at ultra-high intensity laser irradiation and the impact of density oscillation

To cite this article: F Paschke-Bruehl *et al* 2023 *New J. Phys.* **25** 043024

View the article online for updates and enhancements.

You may also like

- Review of laser-driven ion sources and their applications
Hiroyuki Daido, Mamiko Nishiuchi and Alexander S Pirozhkov
- Freezing water simulations in isochoric systems – preliminary analysis
G A Bechea, I Câmpean, L M Scutaru et al.
- CHARACTERIZING TRANSITION TEMPERATURE GAS IN THE GALACTIC CORONA
Bart P. Wakker, Blair D. Savage, Andrew J. Fox et al.

This content was downloaded from IP address 131.169.135.205 on 22/05/2023 at 09:00

IOP Publishing New J. Phys. 25 (2023) 043024 https://doi.org/10.1088/1367-2630/accdfa

New Journal of Physics
The open access journal at the forefront of physics

Deutsche Physikalische Gesellschaft DPG
IOP Institute of Physics

Published in partnership with: Deutsche Physikalische Gesellschaft and the Institute of Physics

OPEN ACCESS

RECEIVED
28 November 2022

REVISED
21 March 2023

ACCEPTED FOR PUBLICATION
18 April 2023

PUBLISHED
27 April 2023

Original Content from this work may be used under the terms of the Creative Commons Attribution 4.0 licence.

Any further distribution of this work must maintain attribution to the author(s) and the title of the work, journal citation and DOI.

PAPER

Heating in multi-layer targets at ultra-high intensity laser irradiation and the impact of density oscillation

F Paschke-Bruehl[1,*], M Banjafar[2], M Garten[1,3,5], L G Huang[1], B E Marré[1], M Nakatsutsumi[2], L Randolph[2,4], T E Cowan[1,3], U Schramm[1,3] and T Kluge[1]

[1] Helmholtz-Zentrum Dresden-Rossendorf, Bautzner Landstraße 400, 01328 Dresden, Germany
[2] European XFEL, Holzkoppel 4, 22869 Schenefeld, Germany
[3] Technische Universität Dresden, 01069 Dresden, Germany
[4] Department Physik, Universität Siegen, 57072 Siegen, Germany
[5] Now with Lawrence Berkeley National Laboratory, 1 Cyclotron Rd, Berkeley, CA 94720, United States of America.
[*] Author to whom any correspondence should be addressed.

E-mail: f.paschke-bruehl@hzdr.de

Keywords: multi-layer target, denstiy oscillation, isochoric heating, plasma heating, buried layer, PIC simulation

Abstract

We present a computational study of isochoric heating in multi-layered (ML) targets at ultra-high intensity laser irradiation ($\sim 10^{20}\,\mathrm{W\,cm^{-2}}$). Previous studies have shown enhanced ion heating at interfaces, but at the cost of large temperature gradients. Here, we study ML targets to spread this enhanced interface heating to the entirety of the target and find heating parameters at which the temperature distribution is more homogeneous than at a single interface while still exceeding the mean temperature of a non-layered target. Further, we identify a limiting process of pressure oscillations that causes the layers to alternate between expanding and being compressed and leads to lower ion temperatures. Based on that, we derive an analytical model estimating the oscillation period to find target conditions that optimize heating and temperature homogeneity. This model can also be used to infer the electron energy from the oscillation period which can be measured e.g. by XFEL probing.

1. Introduction

Studying solids upon high-intensity laser irradiation allows to observe and learn about plasma dynamics that have impact on a wide variety of applications such as tumor therapy [1–4], fusion research [5–8] or laboratory astrophysics [9, 10]. Previous studies have shown, that a specific target design can optimize the laser-target interaction towards preferred mechanisms like rear particle acceleration [11, 12], front surface compression [13–15] or bulk heating [16, 17]. Following this approach, we present a computational study of multi-layered (ML) targets to study and enhance specifically the target heating. We show that ML targets can be an useful tool for ultra high energy density (UHED) experiments using high-power short pulse lasers, because ions can reach temperatures around 1 keV. Such high temperatures allow to reproduce exotic states of matter, as they appear in the far corners of our Universe, in laboratories on earth [18]. ML targets could reproduce states that occur in stellar crusts, planetary cores or cooling white dwarfs [19]. Further, ML targets enable the investigation of valuable properties of UHED plasmas such as reflectivity, transmission [20] and XUV/x-ray opacity [21], which helps interpreting the optical signals detected by telescopes and thus learn about astrophysical phenomena. Additionally, states with such high pressure are required in fast ignition or inertial confinement fusion implosions [22, 23].

There are several processes known to transfer energy from the laser to bulk temperature, e.g. isochoric heating by particle acceleration at the front surface [24–26], subsequent heat diffusion [26, 27], shocks [28, 29], or in the case of ultra-intense lasers also return current generation balancing the dense relativistic electron beam accelerated by the laser [17, 30–32]. The latter usually dominates the heating for short time scales (100 s fs) and has the advantage of relatively homogeneous heating through the target compared to diffusion or shocks. Nevertheless, heating by laser accelerated electrons has been found to be most efficient at

© 2023 The Author(s). Published by IOP Publishing Ltd on behalf of the Institute of Physics and Deutsche Physikalische Gesellschaft

interfaces, as derived in [33]. The simulation study by Huang *et al* (2013) has shown, that ion heating at a buried interface between two materials can increase the temperatures by more than a factor of two compared to a pure material, because of a TNSA-like (target normal sheath acceleration) expansion at the interface. However, the downside of such heating is an inhomogeneous heat distribution over the target, since only in the small volume—within a Debye length—around the interface does the enhanced heating occur. This motivates the present study to investigate ML targets, aiming at combining efficient *and* homogeneous heating. In the ML target we stack multiple interfaces behind each other to spread the enhanced interface heating to the entire target depth.

Previous experimental studies that investigate isochoric heating in solid targets employ single layers as tracers for spectroscopy to measure the bulk temperature [34–36]. Further, there are multiple experimental studies that investigate the heating of homogeneous, single material targets and studies investigating ML targets [37, 38]. However, the interface effect and its impact on heating have not been discussed in an experimental context yet, which is why we want to establish them for future lab studies.

Additionally, in the case of ML targets we observe complex dynamics of oscillating layer densities, occurring as a result of the layered target geometry and high electron energy T_e, dynamics that also affect the ion heating. Based on that, we present an analytic model for the oscillation period ω_{osc} to predict optimal heating conditions, considering limiting quantities, such as ML layer thickness and density. The model draws a connection between layer oscillation frequency ω_{osc} and electron energy T_e which could be employed to measure T_e by detecting and measuring the oscillation frequency, e.g. by time-resolved XFEL (x-ray free-electron laser) scattering [39].

2. Results

2.1. Setup

We performed 2D3V simulations (2 dimensional in space, 3 dimensional in velocity) to compare ML targets with different number of layers, as seen in figure 1, using the particle-in-cell code SMILEI [40]. We focus on an exemplary target, made of copper and aluminum layers with a 150 nm front surface copper shield (cp. dashed white line in figure 1) to protect the ML structure and ensure similar laser absorption for all cases. While varying the number of layers n_l, the layer thicknesses are adjusted so that the total target thickness is kept roughly constant at $d_{\mathrm{tot}} \simeq 1 - 1.1\,\mu$m.

The laser parameters in the simulations, if not stated otherwise, are peak intensity $I_L = 10^{20}\,\mathrm{W\,cm^{-2}}$, pulse duration $\tau_{\mathrm{FWHM}} = 40\,$fs (temporal Gaussian profile, plane wave, linear polarization in y-direction, laser propagation in x-direction), typical parameters e.g. for Ti:sapphire laser systems. Accordingly, we set the laser wavelength to 800 nm (see Methods for complete computational parameters). All times will be given relative to the arrival of the laser pulse maximum on the target surface.

As we will discuss ion heating in the following sections, it is important to clarify the meaning of the term T_i in the simulation: as ion temperature we define the average kinetic energy of ions derived from their thermal momentum in z-direction only, thus $T_i = \bar{p}_z^2/2m_i$. Since our simulations are 2D simulations and the laser is polarized in y-direction, ions gain momentum in z-direction only via collisions. Hence, T_i as defined above consists only of energy due to particle interactions and excludes directed energy caused by longitudinal or transverse movement from acceleration by the laser (linear polarization in y-direction, laser propagation in x-direction). Therefore, T_i, as we define it, corresponds to a real plasma temperature. Further, we will use the average electron kinetic energy $T_e = (\bar{\gamma}_e - 1)m_e c^2$ with $\bar{\gamma}_e$ being the average electron Lorentz factor in x-direction, i.e. laser propagation direction. For thermalized electrons this is equal to the temperature, but especially in early times the quantity also includes directed non-thermal energy from the laser acceleration.

If not stated otherwise, all units are normalized to m_e, c, e, ω and the critical plasma density $n_c = \epsilon_0 m_e \omega_L^2/e^2$ with vacuum permittivity ϵ_0 and laser frequency ω_L.

2.2. Heating in ML targets

First, we investigate the ion heating in the embedded copper layers in figure 2, showing the evolution of the copper temperature T_i for a homogeneous target compared to ML targets with 1, 5 and 10 layers of each material, respectively. We observe an enhancement of temperature close to the interfaces for all cases, most dominant for the cases $n_l = 1$ and $n_l = 5$. This local interface heating occurs because of an expansion of the denser material (copper) into the less dense material (aluminum), induced by a pressure difference. The expansion mechanism is comparable to the well known process of TNSA, where electrons that expand into vacuum cause an electric field, which drag the ions with them. Here, ions expand into the lower density layer instead of vacuum, but also gain momentum, i.e. directed forward movement due to the electric field caused by the expanding electrons, as we see in detail in figure 3 and as predicted in [33]. Due to the expansion and thus forward movement, ions collide, leading to a conversion of kinetic energy into thermodynamic heat and

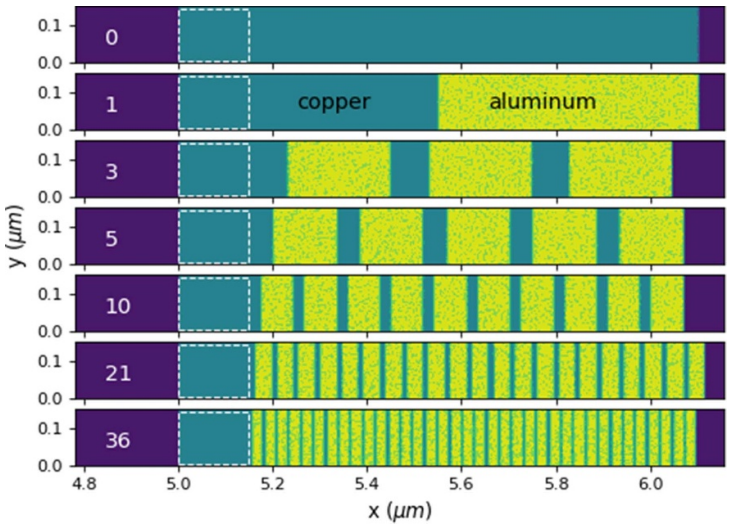

Figure 1. Target setup in the simulations with varying number of layers $n_l = \{0, 1, 3, 5, 10, 21, 36\}$ (top to bottom) and 150 nm copper shield (dashed, white line). Laser is incoming from the left.

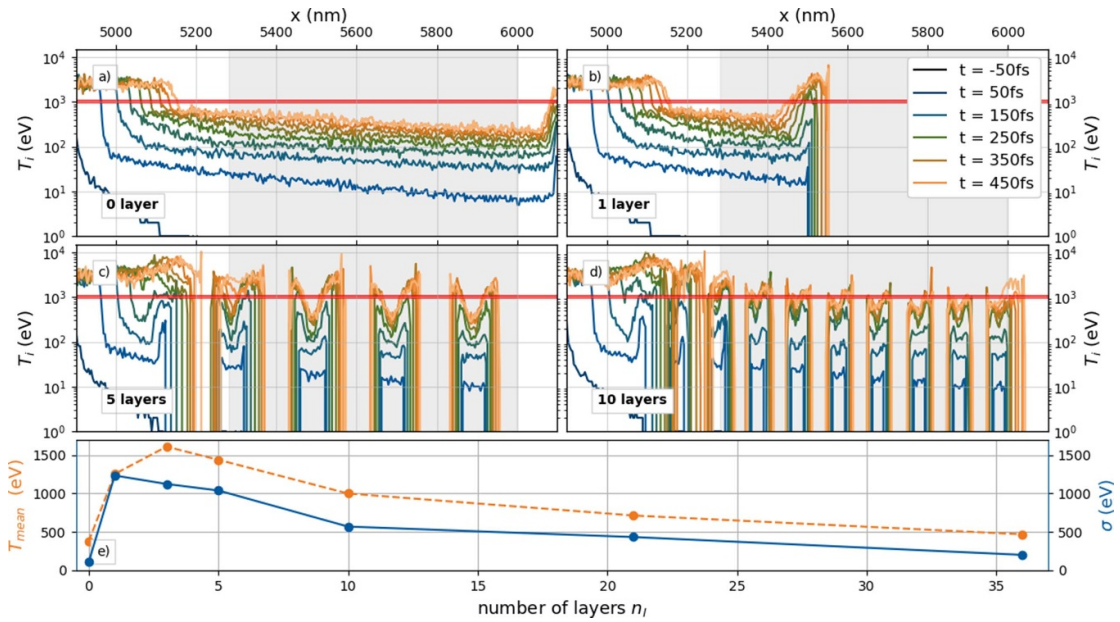

Figure 2. (a)–(d) Temperature of copper ions T_i in the target over time for $n_l = \{0, 1, 5, 10\}$ layers with time relative to the arrival of the temporal peak of the laser pulse on the target surface. (e) Mean ion temperature (orange, dashed) and its variation (blue) in the ML region (shaded area).

thus increased ion temperature compared to target regions where no expansion occurs and heating happens only by electron-ion collisions. For a larger number of layers the temperature starts to decrease, while the average throughout the target bulk always remains higher than in the homogeneous non-layered target (figure 2(e), orange line).

In particular in figure 2(e) (blue line) we recognize that more layers cause a lower temperature spread through the target depth. This observation can be explained easily: more layers cause the expansion to happen all over the target and thus decrease the temperature spread between two regions, also seen by comparing figures 2(b) and (d).

At the same time we observed a decrease in temperature when increasing the number of layers beyond $n_l = 5$ for our specific target parameters. This heating deficit can be explained by a competing process of oscillating layer densities, which is the topic of the remainder of this paper. The oscillations cause the aforementioned expansions at the interfaces to decelerate and ultimately reverse due to reversing pressure relations of neighboring layers. This causes the particle momenta to reduce, and thus collisionality and

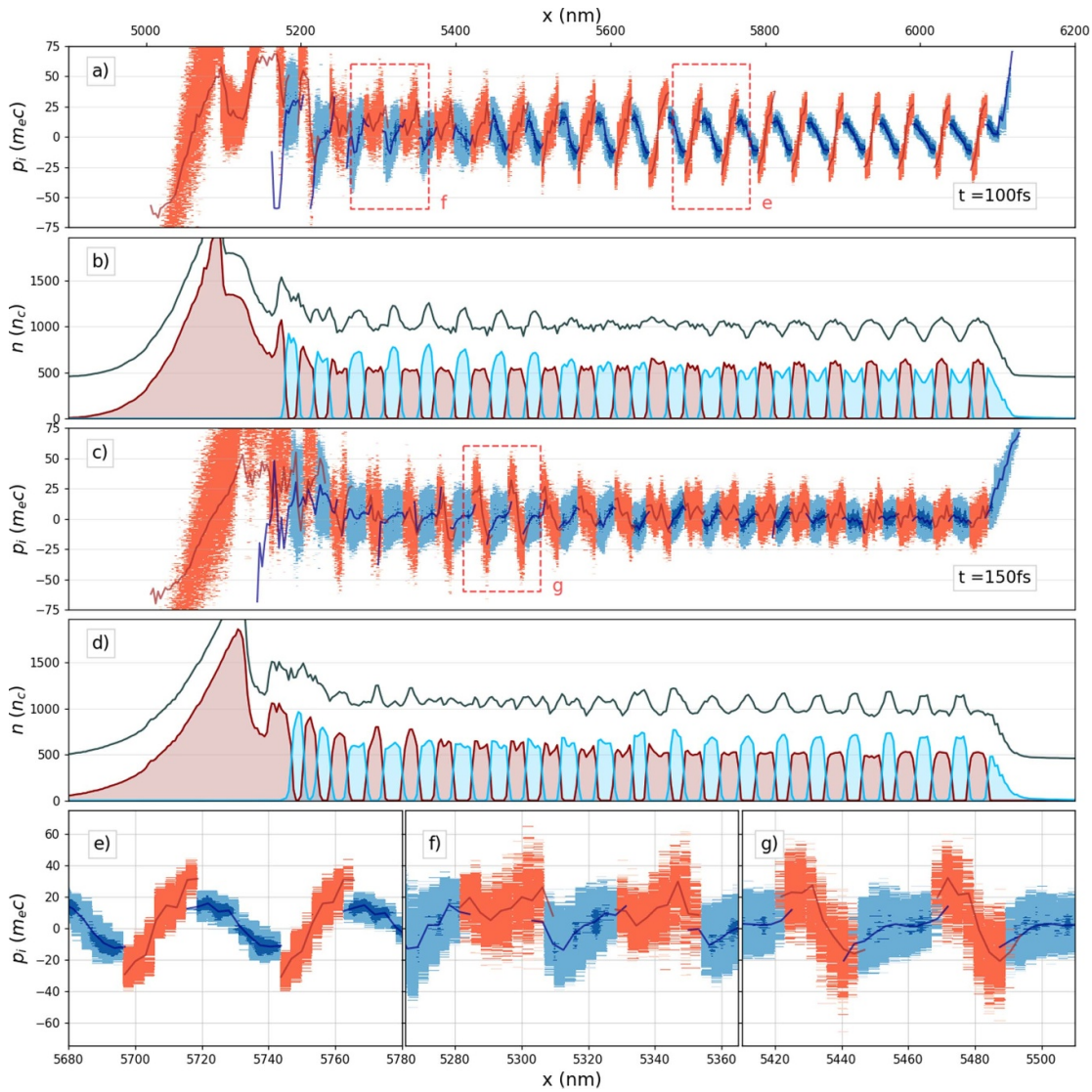

Figure 3. (a) Phase space of copper (orange) and aluminum (blue) at $t = 100$ fs for $n_l = 21$ with p_x in laser direction. (b) Charge density at $t = 100$ fs and free electron density (grey) with offset. (c) Phase space at $t = 150$ fs. (d) Charge density at $t = 150$ fs and free electron density (grey) with offset. (e) Phase space at $t = 100$ fs. (f) Phase space at $t = 100$ fs. (g) Phase space at $t = 150$ fs. Momentum is given in $m_e c$ and density is given in units of critical plasma density n_c.

heating to behave likewise. This leads to a decrease in temperature in comparison to a single interface, where no oscillation appears, i.e. where particles expand freely without reversion of momenta.

The optimum between the highest temperature (i.e. less interfaces) and a homogeneous temperature distribution (i.e. more interfaces) is around $n_l = 10$ layers in our case, where the mean temperature is up by a factor of more than 2 compared to the homogeneous plasma and the temperature spread has already dropped to less than half of that in the single interface case.

In the following we will give an analytic description of the density oscillations in order to find a general expression for optimum parameters.

2.3. Density oscillation

In this section we want to understand and describe the aforementioned oscillation of layer densities in detail to further estimate its impact on the heating. Figure 3 shows the phase space and density of copper (red) and aluminum (blue) over target depth for the case $n_l = 21$ and $t = 100$ fs ((a), (b)), as well as $t = 150$ fs ((c), (d)). In panels ((e)–(g)) we additionally zoom into the phase space behavior to show the different stages of the copper layer, i.e. expansion (e), turning point (f) and compression (g).

The initial expansion of the copper layers, as in ((e), orange), occurs because of the higher electron density and thus higher pressure compared to the neighboring aluminum layers. This simultaneously leads to a compression of the aluminum layers, see ((e), blue), which causes them to increase in density. With the copper layer decreasing in density due to the expansion, the density and thus pressure relation between the

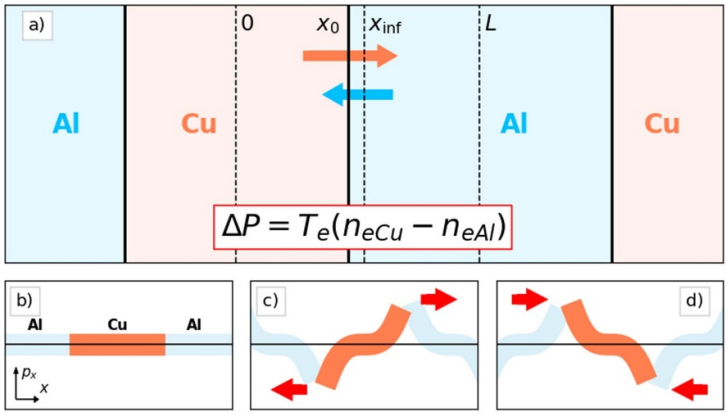

Figure 4. (a) Modeling of layers in the target and plasma pressure for Cu|Al target. We neglect the ion temperature when calculating the pressure difference. (b) Layer standing still. (c) Cu layer (orange) expands due to higher plasma pressure than neighboring aluminum layers (blue). (d) Cu layer is being compressed due to increased plasma pressure of neighbors.

materials slowly reverses, causing the dynamic to decelerate and invert, as seen in (f) and (g). The layers thus repeatedly oscillate in density—and also thickness - , the latter visible in panels (b) and (d).

As explained above, the reversion of the expansion, and thus ion momenta and collisionality, causes a heating deficit in comparison to a pure interface expansion. This leads to a condition for high plasma temperature: half of an oscillation period (i.e. the time to the first reversion of momenta) shall be large compared to the heating time (i.e. the time until half of the maximum temperature is reached), $T_{\mathrm{osc}}/2 \gg \tau_H$, so that momenta do not reverse during the heating process and hence do not cause a heating deficit. In the following we derive a simple analytic expression for the oscillation period T_{osc} for a given material and layer thickness to later use in the heating context. First of all, the driving force of the oscillation is the pressure difference between layers, or specifically the difference in free electron density. The motion is caused by an overshooting, due to ion inertia, of the expanding/compressing motion compensating the pressure difference.

When looking at the density profiles in figure 3, particularly the free electron density (grey) over time, one might think there is a global density motion through the target, comparable to a pressure wave, but that is not the case. As we will see in the following, the single layers are local oscillators, only dependent on local density and electron energy. Since we are only interested in longitudinal forces (x-direction), we can reduce our analysis to 1 dimension. We start with the plasma pressure in two neighboring layers with index j and $j+1$

$$P_j = P_{i,j} + P_{e,j} \tag{1}$$

where

$$\begin{aligned} P_{i,j} &= n_{i,j} T_i \\ P_{e,j} &= n_{e,j} T_e \end{aligned} \tag{2}$$

are the ion and (free) electron pressure, respectively, with ion density $n_{i,j}$, free electron density $n_{e,j} \equiv n_j$ and respective temperatures T_e and T_i in layer j.

Initially, electrons are heated faster than ions ($T_e \gg T_i$), because of the mass relations ($m_i \gg m_e$). Therefore $P_{e,j} \gg P_{i,j}$ and we can neglect the pressure induced by ions. Equation (1) then reduces to $P_j = P_{e,j}$.

Assuming the electron energy to be similar in neighboring layers, because the temperature gradient in the target is large compared to the size of the layers, cp. Figure 2, the pressure on the interface is then simply given by $\Delta P = \left(n_j - n_{j+1}\right) T_e$. This pressure leads to a compression of the low density layer (w.r.t. free electrons) and expansion of the high density layer. At some point the low density layer is compressed enough, that as the inert ions continue to move it reaches higher density than the other layer. This reverses the net pressure direction and the process starts again, leading to a continuous oscillation of the layers, see figure 4.

To describe this process quantitatively, we follow the derivation of the oscillation of two gases in a cylinder of length L and separated by a heavy piston, as done by Gislason [41]. We can adapt this model to our conditions by replacing the piston with the heavy bulk ions, so that the pressure primarily acts on them, while the pressure on the electrons is neglected due to their small mass. We now define the virtual ion piston, that can be thought of as the moving mass M, given by the mass of the *moving* ions between the centers of

two neighboring layers. The equation of motion for this virtual ion piston can then be written with the areal force density $\tilde{f}_x = \Delta P(t) = \Delta n(t) T_e$ with $\Delta n(t) = n_j(t) - n_{j+1}(t)$ as

$$\frac{d}{\mathrm{d}t}\left(\tilde{M}X(t)\right) = \Delta n(t) T_e. \tag{3}$$

Here, $\tilde{M}$ is the fraction $g_1\tilde{M}_0$ of moving ions of the total mass density $\tilde{M}_0 = x_0\rho_j + (L - x_0)\,\rho_{j+1}$, $\ddot{X}(t) = g_2\ddot{x}$ is the average acceleration at time t of the moving ions.

To obtain g_1 and g_2, we have to recognize that possibly not all ions are moving (g_1) and that not all ions that are moving do so with the same velocity (g_2). Regarding the former, for thin layer thicknesses as considered here, almost all ions are moving because of the comparably large scale length at the interfaces ($c_s T_{\mathrm{osc}} \simeq 30nm$), so we can set $g_1 \cong 1$. Only for thicker layers is $g_1 < 1$. Secondly, we have to take into account that those ions in motion are moving with a velocity depending on the distance from the center of the layer. The ions exhibit a velocity dispersion that is nearly linear, as can be seen in figure 3. Due to the symmetry of the problem, at the layer center the ion velocity is always zero, while at the interface it is at its maximum value $\dot{x}(t)$. We therefore apply the approximation for the average velocity of the moving ions at time t: $g_2 \equiv \dot{X}/\dot{x} \cong 0.5$.

As shown in figure 4, the initial thickness of odd numbered layers j is $2x_0$ and that of even numbered layers $j+1$ is $2\,(L - x_0)$ and their interface at time t is positioned at $x(t)$ with $x(0) = x_0$. The average free electron densities inside the respective layers are then connected with the momentary interface position by

$$\begin{aligned} n_j(t) &= n_j^0 \frac{x_0}{x(t)} \\ n_{j+1}(t) &= n_{j+1}^0 \frac{L - x_0}{L - x(t)}. \end{aligned} \tag{4}$$

Equation (3) can then be written as

$$\tilde{M}_0\ddot{x} \cong 2T_e\left(n_j^0 \frac{x_0}{x_\infty + \Delta x} - n_{j+1}^0 \frac{L - x_0}{L - x_\infty - \Delta x}\right) \tag{5}$$

where $\Delta x \equiv x - x_\infty$ and x_∞ is the equilibrium position where $P_j = P_{j+1}$, so $\tilde{f}_x = 0$ with equation (4),

$$x_\infty = L \cdot \left[1 + \frac{n_{j+1}^0 (L - x_0)}{n_j^0 x_0}\right]^{-1}. \tag{6}$$

We can now perform a Taylor expansion on the right hand side of equation (5) for small values of $\Delta x \ll x_\infty$ and obtain $\ddot{x} = -\Delta x \omega_{\mathrm{osc}}^2$ with oscillation frequency $\omega_{\mathrm{osc}} = \frac{2\pi}{T_{\mathrm{osc}}}$ and oscillation period T_{osc}. Then we obtain

$$\omega_{\mathrm{osc}}^2 = \frac{2T_e}{\tilde{M}_0}\left[n_j^0 \frac{x_0}{x_\infty^2} + n_{j+1}^0 \frac{(L - x_0)}{(L - x_\infty)^2}\right]. \tag{7}$$

For thicker foils, where $g_1 < 1$, equation (7) resembles the lower limit for the oscillation frequency.

The oscillation frequency as derived above depends on three fundamental quantities: the layer thicknesses, the layer composition (ion/electron densities and masses) and the electron energy.

With equation (7) the oscillation period is expected to increase with increasing areal mass density and decrease with T_e, so the layers oscillate slower for heavier materials, but faster for higher temperatures. To further investigate the latter dependency we performed additional simulations, this time varying laser intensity. These simulations contain tantalum and copper nitrite layers, similar geometry to the setup in figure 1 for $n_l = 21$.

Figure 5 shows the density over time for different tantalum layer, varying either their position in the target or the laser intensity and thus the local electron energy. We see that higher laser intensities and positions further to the front, i.e. higher T_e, cause shorter oscillation periods, as expected from equation (7). Further, we can measure T_{osc} and compare to equation (7), as shown in figure 6. There we show the oscillation period in dependence of the temperature. The agreement of the analytic model and the simulations is surprisingly good, considering that we take only the average layer motion into account and neglect any damping terms in equation (7).

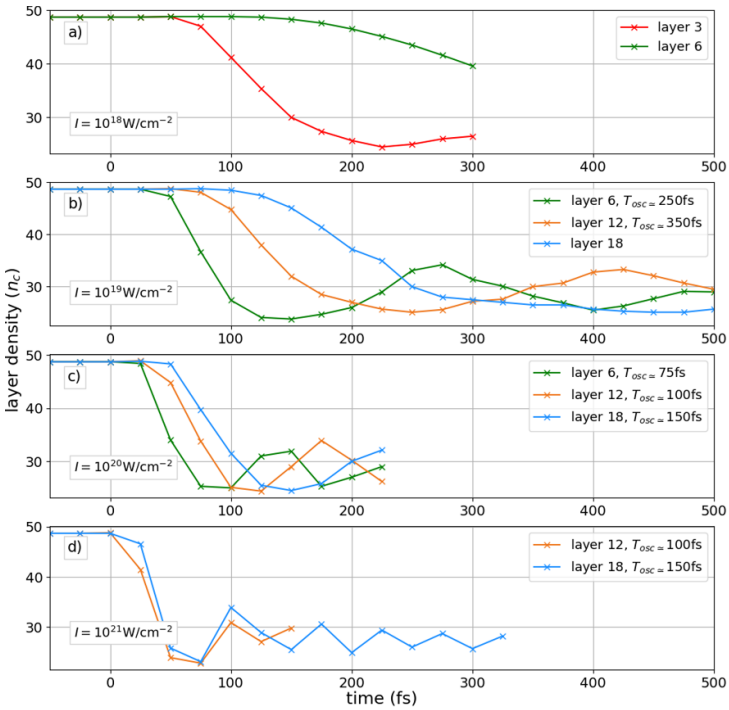

Figure 5. Density of tantalum layer over time for Ta|Cu_3N target and $n_l = 21$ for different layer positions (green line at 6th layer (front), orange at 12th (center), blue at 18th (rear)) and laser intensities ((a) 10^{18} W cm^{-2}, (b) 10^{19} W cm^{-2}, (c) 10^{20} W cm^{-2}, (d) 10^{21} W cm^{-2}), both affecting the electron energy in the layer. The density measurement in (c) and (d) is stopped by the compression wave reaching the according layer from the front, i.e. destroying the layer structure..

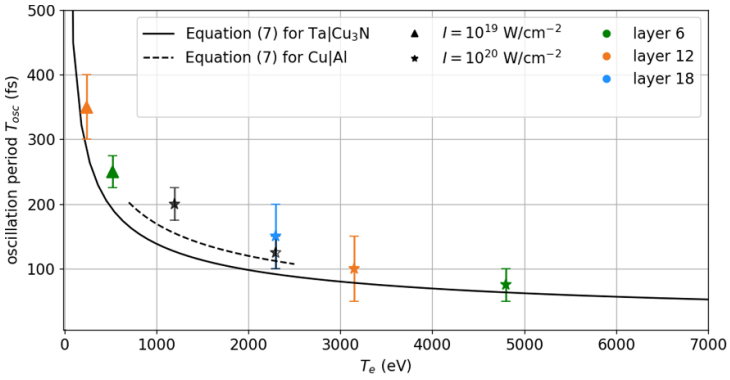

Figure 6. Comparison of oscillation period (equation (7)) and simulation results for tantalum and copper nitrite target. For the energy T_e only momenta in x-direction, i.e. momenta causing pressure in x-direction and thus at the interface, are considered.

2.4. Optimal heating

We can now use the derivations above to obtain an approximate condition for optimal heating in an ML target. First, we require that the expansion of the layer of interest shall be equal or larger than half the neighboring layer thickness, i.e.

$$c_s\tau > x_0 \tag{8}$$

so that the enhanced heating happens in the entirety of the layer and thus ensure homogeneous heating. Here, $c_s \cong \left(T_e Z/M_j\right)^{1/2}$ is the ion sound speed with ion charge Z and ion mass M_j, τ is the expansion time, i.e. the smaller of either half of the oscillation period or (for thick layers) the heating time, $\tau = \min\left[T_{\mathrm{osc}}/2, \tau_H\right]$ [42].

In addition to that we require half of the oscillation period, i.e. until the first turning point, to exceed the heating time to ensure an advantage in heating in comparison to a non-layered target, as discussed before. This brings

$$T_{\mathrm{osc}}/2 > \tau_H. \tag{9}$$

We can now make an estimation for the copper and aluminum target above and compare to figure 2. The average electron energy inside the bulk during the first oscillation for our laser conditions is approx. $T_e \approx 1.1\,\mathrm{keV}$ and with $Z/M_{\mathrm{Cu}} \approx (2m_p)^{-1}$ and a oscillation period of $\tau \approx 150\,\mathrm{fs}$ condition (8) can be evaluated for the copper layer thickness to $d_{\mathrm{Cu}} \leqslant 70$ nm. We defined $d_{\mathrm{Al}} = 2.6 d_{\mathrm{Cu}}$, hence the only free parameter is L, or in other words n_l. In the $d = 850$ nm thick ML region of the target we therefore require more than $n_l = d/(d_{\mathrm{Cu}} + d_{\mathrm{Al}}) \cong 3$ layers of each copper and aluminum. At the same time condition (9) can be evaluated for an approximate heating time in our conditions of $\tau_H \approx 200\,\mathrm{fs}$ (cp. figure 2) and equation (7) to $n_l \leqslant 8$. As can be seen in figure 2(e), this is exactly the range where the homogeneity of the temperature rapidly improves while the average temperature is still much higher than in the homogeneous target.

3. Discussion and conclusion

We performed simulations of ML targets and studied the isochoric heating in the embedded layers. Further, we successfully expanded the enhanced interface heating, as stated in [33], to the entirety of the target and discovered a limiting effect on the heating—the density oscillation. The derived analytic expression for the oscillation period shows good agreement with the 2D3V particle-in-cell simulations. Based on the analytic expression for the oscillation period, we can derive a ML target setup for optimal heating, exceeding the temperatures of a homogeneous target. Finally, we want to highlight that the ML structure is not only advantageous for enhanced heating of the embedded layers, but it can also serve as a diagnostic tool e.g. for GISAXS (grazing-incidence small-angle x-ray scattering), as done in [39]. GISAXS allows to estimate the densities in the layers, as the x-ray scattering pattern changes with the layer quantities, so one could infer the oscillation frequency and thus calculate the local electron energy without any further assumptions. Though the temperature can be inferred spectroscopically or from x-ray Thomson Scattering (XRTS) including novel, essentially model free schemes for homogeneous plasmas [43], those methods rely on complicated atomic physics in modeling the radiative properties of warm and hot dense matter (spectral methods), or average over the full depth of the target (XRTS). Hence a submicron temperature resolution needs careful future theoretic modeling and is beyond the scope of the current state-of-the-art. Here, buried ML structures as proposed above could pose a possible alternative. Buried ML structures at different depths could be used to investigate the depth heating profile with GISAXS.

4. Methods

4.1. Computational parameters

The special simulation geometry is semi 2D, describing a two dimensional (x, y) box with very small spread in transverse direction. The simulation box measures $0.15 \times 10\ \mu$, i.e. 48 cells in x direction (laser-longitudinal), 3200 cells in y direction (laser-transverse) and a resolution of 256 cells per laser wave length ($\lambda = 0.8\mu$m). According to the CFL-condition (Courant-Friedrichs-Lewy), the time resolution was set to 356 time steps per laser period. Further, we assigned 65 particles per cell for each material (electrons, ions).

Data availability statement

The data that support the findings of this study will be openly available following an embargo at the following URL/DOI: https://rodare.hzdr.de/.

Author contributions

Conceptualization and writing—original draft preparation F P-B, T K; draft review T K, B E M, M G; simulations and data-analysis F P-B; subject specific comments and support L R, L G H, M N, M B; project administration T E C, U.S. All authors have read and agreed to the published version of the manuscript.

ORCID iDs

F Paschke-Bruehl https://orcid.org/0009-0001-0047-1051
M Garten https://orcid.org/0000-0001-6994-2475
M Nakatsutsumi https://orcid.org/0000-0003-0868-4745
U Schramm https://orcid.org/0000-0003-0390-7671
T Kluge https://orcid.org/0000-0003-4861-5584

References

[1] Kraft S D *et al* 2010 Dose-dependent biological damage of tumour cells by laser-accelerated proton beams *New J. Phys.* **12** 085003
[2] Zeil K *et al* 2013 Dose-controlled irradiation of cancer cells with laser-accelerated proton pulses *Appl. Phys.* B **110** 437
[3] Karsch L, Beyreuther E, Enghardt W, Gotz M, Masood U, Schramm U, Zeil K and Pawelke J 2017 Towards ion beam therapy based on laser plasma accelerators *Acta Oncol.* **56** 1359
[4] Kroll F *et al* 2022 Tumour irradiation in mice with a laser-accelerated proton beam *Nat. Phys.* **18** 316
[5] Kodama R *et al* 2001 Fast heating of ultrahigh-density plasma as a step towards laser fusion ignition *Nature* **412** 798
[6] Roth M *et al* 2001 Fast ignition by intense laser-accelerated proton beams *Phys. Rev. Lett.* **86** 436
[7] Fernandez J C, Albright B J, Beg F N, Foord M E, Hegelich B M, Honrubia J J, Roth M, Stephens R B and Yin L 2014 Fast ignition with laser-driven proton and ion beams *Nucl. Fusion* **54** 054006
[8] Zylstra A B *et al* 2021 Record energetics for an inertial fusion implosion at NIF *Phys. Rev. Lett.* **126** 025001
[9] Bulanov S V, Esirkepov T Z, Habs D, Pegoraro F and Tajima T 2009 Relativistic laser-matter interaction and relativistic laboratory astrophysics *Eur. Phys. J.* D **55** 483
[10] Bulanov S V, Esirkepov T Z, Kando M, Koga J, Kondo K and Korn G 2015 On the problems of relativistic laboratory astrophysics and fundamental physics with super powerful lasers *Plasma Phys. Rep.* **41** 1
[11] Snavely R A *et al* 2000 Intense high-energy proton beams from petawatt-laser irradiation of solids *Phys. Rev. Lett.* **85** 2945
[12] Maksimchuk A, Gu S, Flippo K, Umstadter D and Bychenkov A Y 2000 Forward ion acceleration in thin films driven by a high-intensity laser *Phys. Rev. Lett.* **84** 4108
[13] Macchi A, Cattani F, Liseykina T V and Cornolti F 2005 Laser acceleration of ion bunches at the front surface of overdense plasmas *Phys. Rev. Lett.* **94** 165003
[14] Mishra R, Sentoku Y and Kemp A J 2009 Hot electron generation forming a steep interface in superintense laser-matter interaction *Phys. Plasmas* **16** 112704
[15] Gaus L *et al* 2020 Probing ultrafast laser plasma processes inside solids with resonant small-angle X-ray scattering (arXiv:2012.07922)
[16] Chawla S *et al* 2013 Effect of Target Material on Fast-Electron Transport and Resistive Collimation *Phys. Rev. Lett.* **110** 025001
[17] Kluge T, Bussmann M, Schramm U and Cowan T E 2018 Simple scaling equations for electron spectra, currents and bulk heating in ultra-intense short-pulse laser-solid interaction *Phys. Plasmas* **25** 073106
[18] Ditmire T *et al* 2004 Overview of future directions in high energy-density and high-field science using ultra-intense lasers *Radiat. Phys. Chem.* **70** 535
[19] Mukai K 2017 X-ray emissions from accreting white dwarfs: a review *Publ. Astron. Soc. Pac.* **129** 062001
[20] Widmann K *et al* 2001 Interferometric investigation of femtosecond laser-heated expanded states *Phys. Plasmas* **8** 3869
[21] Workman J, Nantel M, Maksimchuk A and Umstadter D 1997 Application of a picosecond soft x-ray source to time-resolved plasma dynamics *Appl. Phys. Lett.* **70** 312
[22] Meyer-ter Vehn J 1997 Prospects of inertial confinement fusion *Plasma Phys. Control. Fusion* **39** B39
[23] Edwards C and Danson C 2015 Inertial confinement fusion and prospects for power production *High Power Laser Sci. Eng.* **3** e4
[24] Patel P K, Mackinnon A J, Key M H, Cowan T E, Foord M E, Allen M, Price D F, Ruhl H, Springer P T and Stephens R 2003 Isochoric heating of solid-density matter with an ultrafast proton beam *Phys. Rev. Lett.* **91** 125004
[25] Roth M *et al* 2010 Transport of laser accelerated proton beams and isochoric heating of matter *J. Phys.: Conf. Ser.* **244** 2009
[26] Higashi N, Iwata N, Sano T, Mima K and Sentoku Y 2020 Transition of dominant heating process from relativistic electron beam heating to thermal diffusion in an over picoseconds relativistic laser-solid interaction *High Energy Density Phys.* **37** 100829
[27] Higashi N, Iwata N, Sano T, Mima K and Sentoku Y 2022 Isochoric heating of solid-density plasmas beyond keV temperature by fast thermal diffusion with relativistic picosecond laser light *Phys. Rev.* E **105** 055202
[28] Silva L O, Marti M, Davies J R, Fonseca R A, Ren C, Tsung F S and Mori W B 2004 Proton shock acceleration in laser-plasma interactions *Phys. Rev. Lett.* **92** 015002
[29] Akli K U *et al* 2008 Laser heating of solid matter by light-pressure-driven shocks at ultrarelativistic intensities *Phys. Rev. Lett.* **100** 165002
[30] Glinsky M E 1995 Regimes of suprathermal electron transport *Phys. Plasmas* **2** 2796
[31] Sherlock M, Hill E G, Evans R G, Rose S J and Rozmus W 2014 In-depth plasma-wave heating of dense plasma irradiated by short laser pulses *Phys. Rev. Lett.* **113** 255001
[32] Huang L G, Kluge T and Cowan T E 2016 Dynamics of bulk electron heating and ionization in solid density plasmas driven by ultra-short relativistic laser pulses *Phys. Plasmas* **23** 063112
[33] Huang L G, Bussmann M, Kluge T, Lei A L, Yu W and Cowan T E 2013 Ion heating dynamics in solid buried layer targets irradiated by ultra-short intense laser pulses *Phys. Plasmas* **20** 093109
[34] Eidmann K, Andiel U, Pisani F, Hakel P, Mancini R, Junkel-Vives G, Abdallah J and Witte K 2003 K-shell spectra from hot dense aluminum layers buried in carbon and heated by ultrashort laser pulses *J. Quant. Spectrosc. Radiat. Transfer* **81** 133
[35] Chen S N, Patel P K, Chung H K, Kemp A J, Le Pape S, Maddox B R, Wilks S C, Stephens R B and Beg F N 2009 X-ray spectroscopy of buried layer foils irradiated at laser intensities in excess of 1020 W cm^{-2} *Phys. Plasmas* **16** 1
[36] Hoarty D, James S, Davies H, Brown C, Harris J, Smith C, Davidson S, Kerswill E, Crowley B and Rose S 2007 Heating of buried layer targets by 1ω and 2ω pulses using the HELEN CPA laser *High Energy Density Phys.* **3** 115
[37] Qiu T, Juhasz T, Suarez C, Bron W and Tien C 1994 Femtosecond laser heating of multi-layer metals-II. Experiments *Int. J. Heat Mass Transfer* **37** 2799
[38] Romashevskiy S A, Khokhlov V A, Ashitkov S I, Zhakhovsky V V, Inogamov N A, Komarov P S, Parshikov A N, Petrov Y V, Struleva E V and Tsygankov P A 2021 Femtosecond laser irradiation of a multilayer metal-metal nanostructure *JETP Lett.* **113** 308
[39] Randolph L *et al* 2022 Nanoscale subsurface dynamics of solids upon high-intensity femtosecond laser irradiation observed by grazing-incidence x-ray scattering *Phys. Rev. Res.* **4** 033038
[40] Derouillat J *et al* 2018 SMILEI: a collaborative, open-source, multi-purpose particle-in-cell code for plasma simulation *Comput. Phys. Commun.* **222** 351
[41] Gislason E A 2010 A close examination of the motion of an adiabatic piston *Am. J. Phys.* **78** 995
[42] Mora P 2003 Plasma expansion into a vacuum *Phys. Rev. Lett.* **90** 185002
[43] Dornheim T, Böhme M, Kraus D, Döppner T, Preston T, Moldabekov Z, and Vorberger J 2022 Accurate temperature diagnostics for matter under extreme conditions (arXiv:2206.12805)